Eddy formation near the West coast of Greenland

by

Annalisa Bracco,
Joseph Pedlosky and
Robert S. Pickart

Department of Physical Oceanography,
Woods Hole Oceanographic Institution,
Woods Hole, MA, 02543, USA

Corresponding author address:
Annalisa Bracco
Department of Physical Oceanography,
Woods Hole Oceanographic Institution,
Woods Hole, MA, 02543, USA
E-mail: abracco@whoi.edu

December 22, 2006

Abstract

This note extends the work of Bracco and Pedlosky (2003) investigating eddy formation in the eastern Labrador Sea by including a more realistic depiction of the boundary current. The quasigeostrophic model consists of a meridional, coastally-trapped current with three vertical layers. The current configuration and topographic domain are chosen to match as closely as possible the observations of the boundary current and the varying topographic slope along the West Greenland coast. The role played by the bottom-intensified component of the boundary current on the formation and vertical structure of the Labrador Sea "Irminger Rings" is explored. Results suggest that at the time of formation the eddies are characterized by a strong circulation at depth, possibly allowing for the transport of near-bottom water from the Deep Western Boundary Current into the interior basin. Furthermore this work supports the idea that changes in the vertical current structure could be responsible for the observed variability in the number of the Irminger Rings that are formed and for their characteristics.

1 Introduction

It has been known for some time that an area of high eddy kinetic energy extends from the boundary of the eastern Labrador Sea in the region near 61–62^o N (Heywood et al., 1994; Fig. 1). Recently it has been shown that this feature is associated with the formation of energetic eddies from the boundary current. The eddies subsequently propagate to the southwest and populate the interior of the Labrador Sea (Prater, 2002; Lilly et al., 2003). Various studies have shown that the eddies represent an important flux of heat that helps balance the buoyancy loss through the sea surface during wintertime convection, and, during spring and summer, helps to restratify the basin and modify the newly formed Labrador Sea Water found within it (Lilly et al., 2003; Eden and Böning, 2002; Katsman et al., 2004). A recent investigation of three of those eddies tracked by seagliders hypothesized that they could also be responsible for the annual supply of low salinity waters to the Labrador Sea interior (Hátún et al., 2006), showing that atmospheric fluxes (precipitation minus evaporation) are insufficient to explain the observed seasonal of freshening (Sathiyamoorthy and Moore, 2002).

Both cyclones and anticyclones are spawned from the boundary current, but the anticyclones are longer-lived and hence are found in greater number in the basin. These features are known as Irminger Rings, because of the warm and salty "Irminger Water" found in their cores, and can extend to great depth (deeper than 2km, A. Clarke, personal communication, 2002). Because of their importance to the formation and evolution of Labrador Sea Water—the major mode water of the North Atlantic—the formation mechanism and structure of the eddies must be determined in order to understand fully the mid-depth ventilation of the

subpolar gyre.

The processes leading to formation of the Irminger Rings has been addressed in a series of recent modeling studies. Eden and Böning (2002) with a high resolution ocean general circulation model, and Bracco and Pedlosky (2003) (hereafter BP) with an idealized quasi-geostrophic channel model, suggested that an instability is triggered by the variation in the topography of the continental slope. In particular, the constriction of the isobaths along the West Greenland continental slope, north of Erik Ridge (Fig. 1), induces an enhancement of the eddy kinetic energy. The mechanism for the instability was mainly barotropic according to Eden and Böning (2002), and baroclinic according to BP. Eden and Böning (2002) found that the strength of the Western Greenland Current, influenced by either changes in the wind stress or in the heat flux forcing, was the determining factor for the seasonal changes in eddy kinetic energy of the region. Katsman et al. (2004), using the MIT primitive equation model in an idealized configuration, further explored the sensitivity of the eddy formation to the local bathymetry and the nature of the instability mechanism. They found that the process is mixed, with barotropic energy conversion prevailing in the upper water column, where heat fluxes in winter strengthen the boundary current introducing a seasonal signal in the eddy generation, and baroclinic conversion dominating at depth. This last study, however, neglected the vertical structure of the current system, concentrating on the role of heat-fluxes.

While the detailed structure of Irminger Rings remains largely unknown due to the paucity of observations in this area, some basic features have been identified. Using mooring data from the central Labrador Sea, along with TOPEX/Poseidon altimeter data and limited

hydrography, Lilly et al. (2003) studied the vortex population in the Labrador Sea over the period 1993-1999. They identified and studied 12 Irminger Rings all formed during the period 1997 to 1999. From 1993 to mid-1996 so-called "convective lenses" were observed, with different characteristics and composition, and likely formed in the interior of the Labrador Sea. The Irminger Rings are warm-core anticyclones with a surface-intensified circulation, ranging in radius from 15–30 km, which is significantly larger than the Rossby deformation radius at this latitude (order 10 km). Some of the rings appear to have a "double core" structure with a second velocity maximum at depth (Lilly et al., 2003). While it is presently unknown how common or robust this feature is, it is clear that the eddies have a deep-reaching signature in both density and circulation, and that they may strongly affect the deepest layer of the Labrador Sea.

In the earlier study of BP a two-layer zonal flow was considered, in order to focus on the role of the topography in the generation of the eddies. The Labrador Sea boundary current runs NW-SE at about 40^o and is more aptly represented as a meridional flow in a three-layer system, with the swift West Greenland Current occupying the upper layer, weaker flow at mid-depth, and the bottom intensified Deep Western Boundary Current at the base of the continental slope (Fig. 2). The goal of the present study is to explore the role of the bottom-intensified flow on the instability mechanism and the structure of the Irminger Rings. To do so we consider a three-layer configuration of a simple quasigeostrophic model with the inclusion of meridional, coastally confined currents. The topographic slope, background velocities and the lateral scale of the boundary current are chosen to match as closely as possible the observed boundary current characteristics along the West Greenland

coast. Our focus is on the vertical structure of the vortices at the moment of their formation, in particular on their signature at depth and on the role that the current structure may play at the time of formation. In this work we do not investigate the restratification processes that may take place in those eddies during spring and summer, once they have filled the Labrador Sea interior, and therefore an adiabatic model serves our goal without loss of generality. As shown by Katsman et al. (2004), surface heat fluxes are very important as they introduce a pronounced seasonal cycle by increasing the temperature contrast between the boundary current and the interior of the Labrador Sea at the end of winter. This contrast strengthens the boundary current, as shown by Spall (2004).

Section 2 contains a brief description of the model used. Results are presented in Section 3. In the discussion of Section 4 we explore the possibility, proposed by Lilly et al. (2003), that changes in the current system may be responsible for the interannual and decadal variability of the eddy field off the West coast of Greenland. We also comment on the influence of surface heat fluxes on the vertical structure of the eddies.

2 The model

We consider a baroclinic meridional flow confined in an infinitely long channel of width $L^* = 300km$. The flow is assumed for simplicity to be quasigeostrophic on the beta-plane (see e.g. Pedlosky, 1987).

In the three layer configuration, which, in a first approximation, represents the observed vertical structure of the currents in the region of interest (see Fig. 2), the density is assumed

to be uniform and the horizontal velocities are independent of depth within each layer. We consider for simplicity three layers of equal depth, $H_1 = H_2 = H_3 = 1000m$. (The independence of our results on this assumption has been tested by performing numerical experiments with H_3 varying in the range $H_1 \leq H_3 \leq 1.5H_1$, whereas $H_3 \sim 1.2H_1$ is probably the most relevant to the West Greenland current system).

The equations of motion, nondimentionalized as in BP, are:

$$\frac{\partial Q_i}{\partial t} + J(\psi_i, Q_i) = \nu \nabla^4 \psi_i, \qquad i = 1, 3 \tag{1}$$

where ψ_i is the streamfunction in layer i, $i = 1, 3$; Q_i is potential vorticity given by

$$Q_1 = \nabla^2 \psi_1 - F_1(\psi_1 - \psi_2) + \beta y \tag{2a}$$

$$Q_2 = \nabla^2 \psi_2 - F_2(2\psi_2 - \psi_1 - \psi_3) + \beta y \tag{2b}$$

$$Q_3 = \nabla^2 \psi_3 - F_3(\psi_3 - \psi_2) + \beta y + h(x, y). \tag{2c}$$

ν is the nondimensional coefficient of the horizontal turbulent mixing and J is the Jacobian operator $J(a, b) = \partial_x a \partial_y b - \partial_y a \partial_x b$. The $\nabla^2 \psi_i$ terms are relative vorticity contributions. For three layers of equal depths the interface displacement coefficients F_i are

$$F_1 = F_2 = F_3 = \frac{f_o^2 L_R^2}{g' H} = 1. \tag{3}$$

L_R is the internal Rossby deformation radius used to scale horizontal lengths, while $g' = g\Delta\rho/\rho$ is reduced gravity and f_o is the value of the Coriolis parameter at the central latitude of the domain. In our calculations we assume $L_R = 12km$. $\beta = \beta^* L_R^2 / V$ measures the relative size of the potential vorticity gradient due to planetary differential rotation and

that associated with the vertical shear, with β^* being the dimensional northward gradient of the Coriolis parameter. We take $\beta^* = 1.1 \times 10^{-11} s^{-1} m^{-1}$. The gradient of the Coriolis parameter is small at this scale and latitude and its effects are negligible. In the configuration of relevance to the West Greenland Current similar results are found for $\beta^* = 0$. For completeness, however, it should be mentioned that the presence of β in a meridional channel guarantees the development of the instability independently of the channel width, as shown by Walker and Pedlosky (2002), while a minimum width is required for the instability to take place in the case of a zonal channel (see discussion in BP).

The nondimensional bottom relief is $h(x,y) = \frac{h^* f_o L_R}{v_3^* H_3}$, which contributes to the potential vorticity of the lower layer, where h^* is the dimensional amplitude of the topography and v_3^* is the characteristic (dimensional) along-shelf velocity in the bottom layer. Similarly to BP, the bottom relief has the form

$$h(x,y) = \gamma(y)(x) \ , \tag{4}$$

where γ is a function of the meridional coordinate, y, and x is set to 0 along the western boundary and is equal L at the western wall.

The streamfunction of the flow can be written as

$$\psi_i(x,y,t) = \frac{A_i}{\lambda_i} exp^{-\lambda_i(x)} + \phi_i(x,y,t) \qquad\qquad i = 1,2,3 \tag{5a}$$

where ϕ_i, $i = 1,2,3$ are the perturbation streamfunctions in each layer, A_i are the maximum values of the velocity associated with the vertical shear of the meridional currents, and λ_i^{-1} provides a measure of the width of the currents, set to be $5 \times L_R$ (i.e. 60km in dimensional units) for all layers for simplicity. The current profile requires the coast to be modeled as a

slip boundary, has no inflection points and is, therefore, barotropically stable in the absence of topographic features.

A schematic of the model domain is given in Fig. 3. The steepness of the continental slope varies in the meridional direction in accordance with the observed bathymetry within the dashed box of Fig. 1. Specifically, the average bottom slope as a function of alongslope distance was computed (Fig. 4a), and used to construct a smoothly varying curve that was used in the model (Fig. 4b). We consider a meridional channel of width $L = L^*/L_R$ in nondimensioanal units and we set $\gamma(y)$ to be the positive-definite function shown in Fig. 4b. This essentially divides the channel into three areas: an upstream and downstream region of moderate slope, separated by a region of length a where the slope is strong enough to be considered a vertical wall adjacent to a flat bottom (see Fig.3). Note that the southern transition from moderate to steep slope is less abrupt than the northern transition from steep to moderate slope. (These transitions are hereafter referred to as "steps" that bracket the central region where the bottom is flat). With this choice, the model bathymetry destabilizes the flow in the interval a (see Samelson and Pedlosky, 1990, and BP for more details on the instability analysis).

The average along-shelf velocity of the currents in the three layers are taken to be $v_1^* \sim 12cm/s^{-1}$ for the surface layer, $v_2^* \sim 6cm/s^{-1}$ for the middle one, and $v_3^* \sim 10cm/s^{-1}$ in the bottom layer. (The dependence of the results on the background velocity values is briefly discussed in the following section.)

3 Results

Eq. (1) and its linearized counterpart have been numerically integrated using the pseudo-spectral code described in BP. As in BP, a localized short bottom-trapped wave is responsible for the eddy formation. Here the bottom-trapped wave is present whenever $\frac{\partial q_3}{\partial x} = [+(A_3\lambda^2 - A_3 + A_2) + \gamma(y)]$ changes sign from positive to negative. In a three layer system as the one chosen, with $\gamma(y)$ being a positive definitive function, the contribution to the cross-channel potential vorticity gradient given by the bottom-enhanced boundary current is therefore necessary to the instability, and the velocity profile in the second and third layer must be such that $(A_3\lambda^2 - A_3 + A_2)$ is negative but in absolute value smaller than γ. This indeed allows for the required sign change at the upstream corner of the unstable interval. In order for the instability to take place the presence of a sufficiently strong bottom current -sufficiently stronger than the one in the intermediate layer- is essential. We consider this a major result of this analysis, as no previous studies have singled out the deep component of the boundary current as critical to the formation of Irminger Rings.

Given the orientation of the domain, the short bottom-trapped disturbance reaches maximum amplitude over the upstream topographic step that separates the stable from the unstable interval. As in BP the equilibration of the linear unstable modes produces a dipole in correspondence to the short trapped wave (Fig. 5). The cyclonic component of the dipolar structure is affected by the image vorticity of opposite sign at the wall (see Carnevale et al., 1997 for a description of the "rebound" process). In particular, it is forced downstream and is easily deformed by the shear in the current, which is of the same sign, until it is destroyed.

(This happens in less than a day in our integrations). The anticyclonic part, on the other hand, is free to move downstream over the flat bottom until it reaches the downstream topographic step and detaches from the boundary after about ten days (Fig 6). As part of this detachment process a new cyclone can form, but it is generally weaker and contains water from the coastal boundary current at the location of the detachment (see Fig. 6).

The size of the eddies at the time of formation at the upstream step is determined by the sharpness of the step, as already found in BP with a detailed parameter exploration. The diameter of the anticyclones is of the order of half of the step extension, i.e. ~ 40 km, in agreement with the observations (Fig. 4a). The anticyclonic vortices are essentially barotropic, with the upper layer core larger in radius than the bottom one. This is due to the stabilizing effect of the bottom slope over the edges of the vortices in the lower layer. The rate of formation is of one new anticyclone every $\sim 6-7$ days. Only about 35% of the eddies formed at the upstream step reach the interior of the basin; the others are reabsorbed in the boundary current or undergo merging events.

Performing a sensitivity study, we have found that reducing the difference in the boundary current velocity between the intermediate and bottom layers to half or less of what is presented above alters the stability properties of the flow, causing the vortices that form at the topographic step to be more unstable and less barotropic. Whenever this is the case, the vortices do not survive long enough to penetrate into the interior of the model domain.

A word of caution should be spent on the realism of the model domain in this study: The geometry of the basin is a crude approximation of the eastern side of the Labrador Sea. We concentrated on representing the observed bathymetry in the region where the flow is locally

supercritical (interval a) and we used a simplified representation of the region included in the dashed box in Fig. 1. Outside such a region the differences between the model (an infinite long channel with a stabilizing bottom slope) and the actual bathymetry are significant. In particular we neglect the northwestward veering of the isobaths at the downstream edge of the interval of instability. The proposed mechanism of formation, however, is able to explain the observed extension of the eddy kinetic energy maximum along the coast in the interval a, the localization of the vortices, their radius, their rate of formation, and the energy transfer terms found by Eden and Böning (2002) in their high resolution model of the West Greenland Current. We think, therefore, that despite the simplifications, the mechanism of vortex formation discussed in this work may be of relevance to the Labrador Sea.

4 Discussion and Conclusions

This work generalizes the results obtained by BP in the case of a three-layer meridional current in a north-south channel. Despite the obvious simplifications, the model adopted is able, with realistic choice of the current scales, to reproduce important features of the observed vortex population shed near the western coast of Greenland, including vortex polarity, radius, rate of formation and deep vertical extension throughout the water column. The generation mechanism of stable coherent vortices results from the equilibration of the most unstable mode associated with local baroclinic instability induced by the variable topography (see also Samelson and Pedlosky (1990) and BP). As shown in BP, the bottom-trapped disturbance is responsible for the vortex formation and grows to balance the ambient gradient of potential

vorticity with time variations of relative vorticity. Subsequently the initial dipole rebounds from the slip wall. Only the anticyclonic component survives in the chosen current system, and it penetrates downstream and then into the basin as single vortex or as a member of a new dipole, extracting the cyclonic component from the boundary current at the location of the detachment.

The seasonal variability in the number of Irminger Rings formed and in their surface intensification is believed to be related to the strengthening of surface heat fluxes during the winter season and to the consequent acceleration of the surface current which becomes unstable (Katsman et al., 2004), or to seasonal variations in the strength of the West Greenland Current, influenced by changes in the wind stress (Eden and Böning, 2002). Our model does not attempt to capture any of those characteristics. However, not surprisingly, the inclusion of a thermal damping between the surface and the intermediate layer induces, in a calculation not shown here, a 'barotropization' of the upper two layers and therefore an intensification of the upper layer disturbances, in the direction of the observed vortex population structure.

Irminger Rings have been observed in abundance since 1997, while a different population of vortices filled the Labrador Sea during the four previous years—the so-called convective lenses. Their formation is also associated with a stronger annual cycle in the eddy kinetic energy field along the West Greenland coast, when compared to the previous period (Brandt et al., 2004). A convincing explanation for their appearance is still missing, but has been sought in the interannual variability of the (surface-intensified) West Greenland Current. However, sea surface temperatures along the West Greenland coast were anomalously low in 1997, suggesting a high inflow of polar water, yet were high the following three years (Buch

et al., 2004). Also, surface winds in the same region do not show a clear trend or change during the 1993-2000 period (although it should be borne in mind that the reliability and time resolution of both atmospheric and surface oceanic fields obtained through satellite measurements are limited due to persistent cloud coverage). Hence it is not obvious how interannual changes in the upper-layer flow are related to changes in eddy formation. Interannual variability in both the surface heat fluxes and the wind stress field, that a recent study suggests to cause the variability of the Deep Labrador Current during the last decade (Dengler et al., 2006), could possibly explain the observed changes in the eddy field off the west coast of Greenland, but this hypothesis is difficult to test using the available data.

Our model suggests that the deep components of the boundary current may play a fundamental role in the interannual variability of eddy formation in the Labrador Sea, a hypothesis supported by the laboratory experiments of Wolfe and Cenedese (2006). The eddies formed in our simple quasigeostrophic model are particularly stable and extend very deep in the water column at the time of formation. Their existence, stability and vertical profiles are directly linked to the presence of a boundary current in the deep layer sufficiently stronger than the flow at mid-depth and having an intensity of the same order of magnitude as the upper-layer current. While stressing again that diabatic effects will further contribute to the stability of the upper part of the eddies, possibly reducing the sensitivity to the subsurface currents during their consequent evolution, our work suggests that changes in the production rate and structure of the eddies formed in this region could be associated with variations of the Deep Western Boundary Current. This supports the idea that the variability in the overall subpolar gyre transport and circulation, as documented in e.g. Hátún et al., 2005,

and not only of its surface expression, may be associated with the generation of Irminger Rings. Further work will test the hypothesis that the variability of the subpolar gyre may modulate the formation of Irminger Rings with a circulation model configured to include the subpolar gyre and the Labrador Sea region.

To conclude, we would like to stress the key importance of long and continued observational time series in the Labrador Sea, to monitor both the surface and the deep circulation in a region of great importance for the climate system.

Acknowledgements

We are grateful to Amy Bower, Fiamma Straneo and Jonathan Lilly for useful discussions during the preparation of this manuscript. The authors wish to thank the two referees for their valuable comments that helped improving the clarity of this work

A.B. is supported by WHOI unrestricted funds, J.P. by the National Science Foundation OCE 85108600 and R.P. by 0450658.

References

Bracco, A., and J. Pedlosky, 2003: Vortex generation by topography in locally unstable baroclinic flows. *J. Phys. Oceanogr.*, **33**, 207-219.

Brandt, P., F. A. Schott, A. Funk, and C. S. Martins, 2004: Seasonal to interannual variability of the eddy field in the Labrador Sea from satellite altimetry. *J. Geophys. Res.*, **109**, C02028, doi:10.1029/2002JC001551.

Buch, E., S. A. Pedersen, and M. H. Ribergaard, 2004: Ecosystem variability in West Greenland waters. *Northwest Atlantic Fishery Science*, **34**, art. 2.

Carnevale, G. F., O. U. Velasco Fuentes, and P. Orlandi, 1997: Inviscid dipole-vortex rebound from a wall or coast. *J. Fluid Mech.*, **351**, 75-103.

Cuny, J., P. B. Rhines, P. P. Niiler, and S. Bacon, 2002: Labrador Sea boundary currents and the fate of the Irminger Sea water. *J. Phys. Oceanogr.*, **32**, 627-647.

Dengler, M., J. Fisher, F. A. Schott, and R. Zantopp, 2006: Deep Labrador Current and its variability in 1996-2005. *Geoph. Res. Lett.*, **33**, L21S06, doi:101029:2006GL026702.

Eden, C., and C. Böning, 2002: Sources of eddy kinetic energy in the Labrador Sea. *J. Phys. Oceanogr.*, **32**, 3346-3363.

Hátún H., A. B. Sandø, H. Drange, B. Hansen, and H. Valdimarsson, 2005: Influence of the Atlantic subpolar gyre on the thermocline circulation. *Science*, **309**, 1841-1844.

Hátún H., C. Eriksen, P. B. Rhines, and J. Lilly, 2006: Buoyant eddies entering the Labrador Sea observed with gliders and altimetry. *J. Phys. Oceanogr.*, submitted.

Heywood, K.J., E.L. McDonagh, and M.A. White, 1994: Eddy kinetic energy of the North Atlantic subpolar gyre from satellite altimetry. *J. Geophys. Res.*, **99**, 22,525-22,539.

Katsman, C. A., M. A. Spall, and R. S. Pickart, 2004: Boundary current eddies and their role in the restratification of the Labrador Sea. *J. Phys. Oceanogr.*, **34**, 1967-1983.

Lilly, J. M., F. Schott, K. Lavender, J. Lazier, U. Send, and E. D'Asaro, 2003: Observations of the Labrador Sea eddy field. *Progress in Oceanography*, **59**, 75-176.

Pickart, R.S. and M.A. Spall, 2006: Impact of Labrador Sea convection on the North Atlantic meridional overturning circulation. *J. Phys. Oceanogr.*, accepted.

Prater, M. D., 2002: Eddies in the Labrador Sea as observed by profiling RAFOS floats and remote sensing. *J. Phys. Oceanogr.*, **32**, 411-427.

Pedlosky, J., 1987: *Geophysical Fluid Dynamics*, New York, Springer-Verlag. 710 pp.

Samelson R. M., and J. Pedlosky, 1990: Local baroclinic instability of flow over variable topography. *J. Fluid Mech.*, **221**, 411-436.

Sathiyamoorthy, S., and G. W. K. Moore, 2002: Buoyancy flux at Ocean Weather Station Bravo. *J. Phys. Oceanogr.*, **32**, 458-474.

Spall, M. A., 2004: Boundary current and water mass transformation in marginal seas. *J. Phys. Oceanogr.*, **34**, 1197-1213.

Walker, A., and J. Pedlosky, 2002: Instability of meridional baroclinic currents. *J. Phys. Oceanogr.*, **32**, 1075-1093.

Wolfe C. L., and C. Cenedese, 2006: Laboratory experiments of eddy generation by a buoyant coastal current flowing over variable bathymetry. *J. Phys. Oceanogr.*, **36**, 395-411.

Figure captions

Fig. 1. Distribution of surface eddy speed (color) in the eastern Labrador Sea from Lilly et al. (2003). The dashed box represents the region over which the average bottom slope was computed in Fig. 3a. The location of the World Ocean Circulation Experiment (WOCE) AR7W hydrographic line is marked. The average velocity section of Fig. 2 was computed along the eastern portion of the WOCE AR7W line (see Pickart and Spall, 2006).

Fig. 2. Average velocity of the boundary current system in the eastern Labrador Sea. Solid contours correspond to poleward flow. WGC = West Greenland Current, and DWBC = Deep Western Boundary Current. This is a smoothed version of the velocity field of Pickart and Spall (2006).

Fig. 3. Schematic of the model geometry. The topography and the current configuration destabilizes the flow in the interval denoted by a. The shading boxes UP and DW indicate the two domains zoomed in Fig. 5. $x = 0$ along the eastern boundary.

Fig. 4. (a) Average bottom slope progressing northward along the continental slope of West Greenland, computed within the dashed box in Fig. 1. The scales used in the model are indicated. (b) The average bottom slope profile used in the model.

Fig. 5. Zoomed-in view of the potential vorticity disturbance in the upper, middle and lower layer with the isolines of the bathymetry overlaid in box UP in the schematic of Fig. 3, which corresponds to the interval 50-200 km in Fig. 4. The wall corresponding

to "*Greenland*" is on the right (at $x = 0$) of each panel. The figure shows the formation of an anticyclone at the upstream step. Units are km for both axes.

Fig. 6. Zoomed-in view of the potential vorticity disturbance in the u pper, middle and lower layer with the isolines of the bathymetry overlaid in box DW in the schematic of Fig. 3, which occupies the interval 290-650 km in Fig. 4 and is about 4-times larger that the upstream box. The wall corresponding to "*Greenland*" is on the right (at $x = 0$) of each panel. The anticyclone formed at the upstream step and shown in Fig. 5 ten day s later is detaching from the boundary and is forming a dipole. Units are km for both axes.

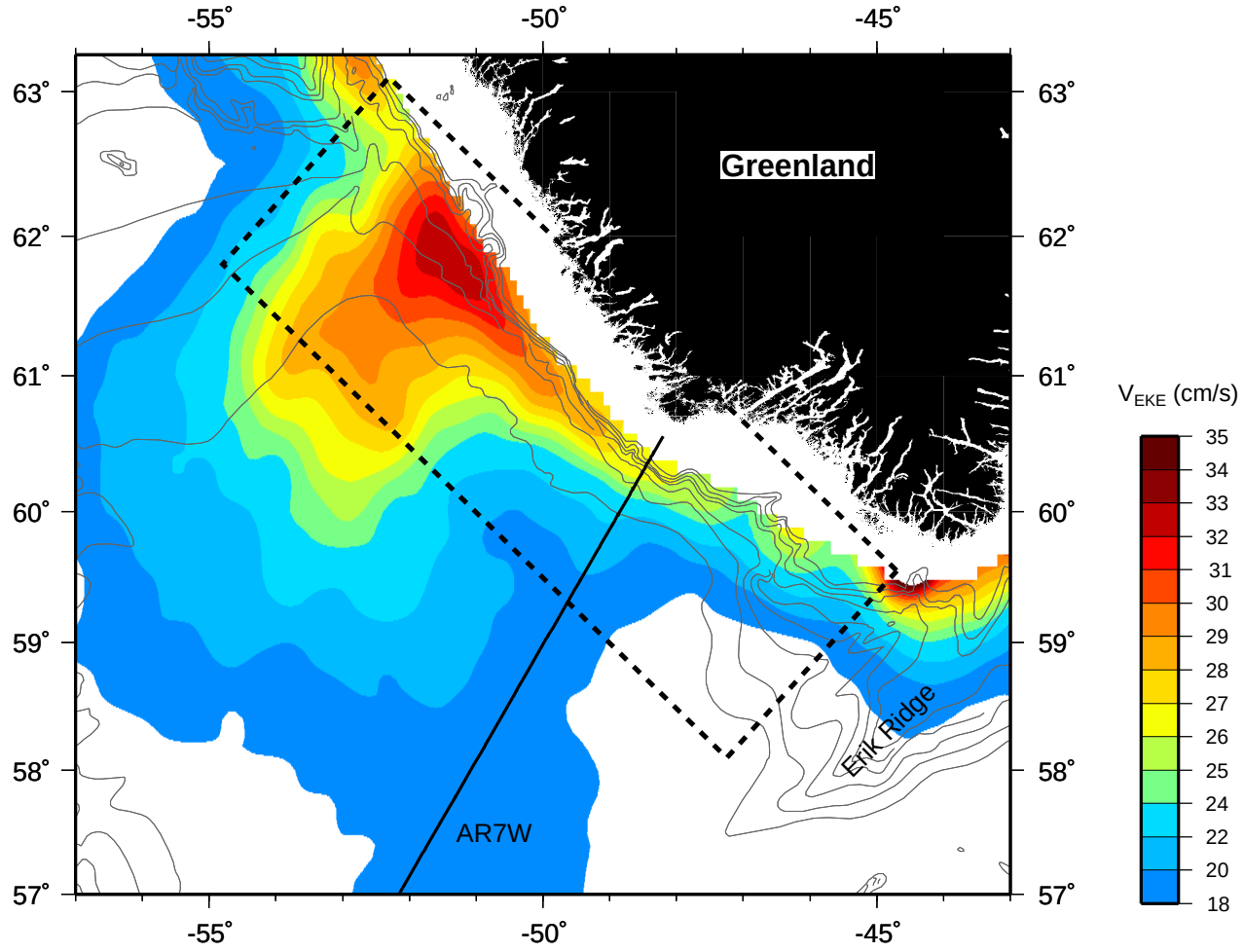

Figure 1: Distribution of surface eddy speed (color) in the eastern Labrador Sea from Lilly et al. (2003). The dashed box represents the region over which the average bottom slope was computed in Fig. 3a. The location of the World Ocean Circulation Experiment (WOCE) AR7W hydrographic line is marked. The average velocity section of Fig. 2 was computed along the eastern portion of the WOCE AR7W line (see Pickart and Spall, 2006).

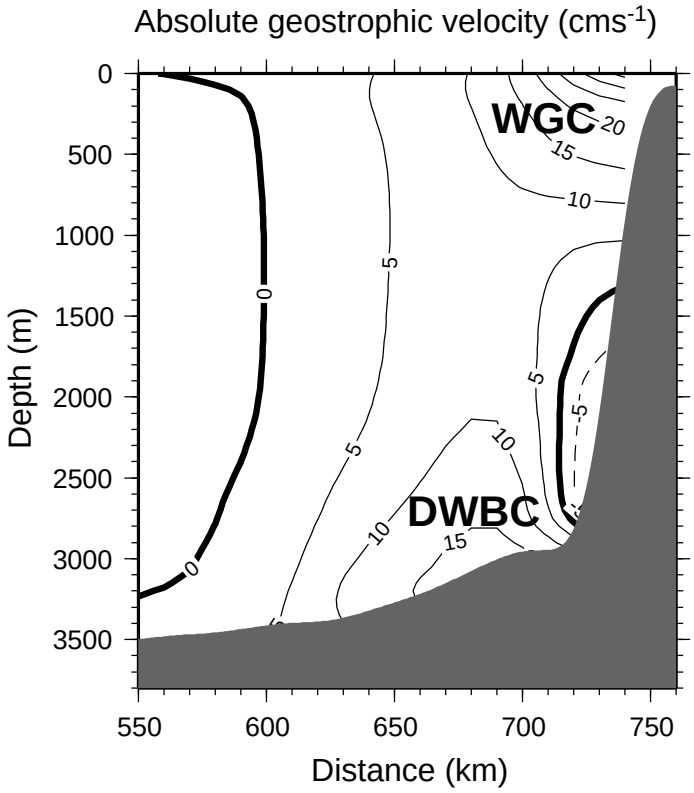

Figure 2: Average velocity of the boundary current system in the eastern Labrador Sea. Solid contours correspond to poleward flow. WGC = West Greenland Current, and DWBC = Deep Western Boundary Current. This is a smoothed version of the velocity field of Pickart and Spall (2006).

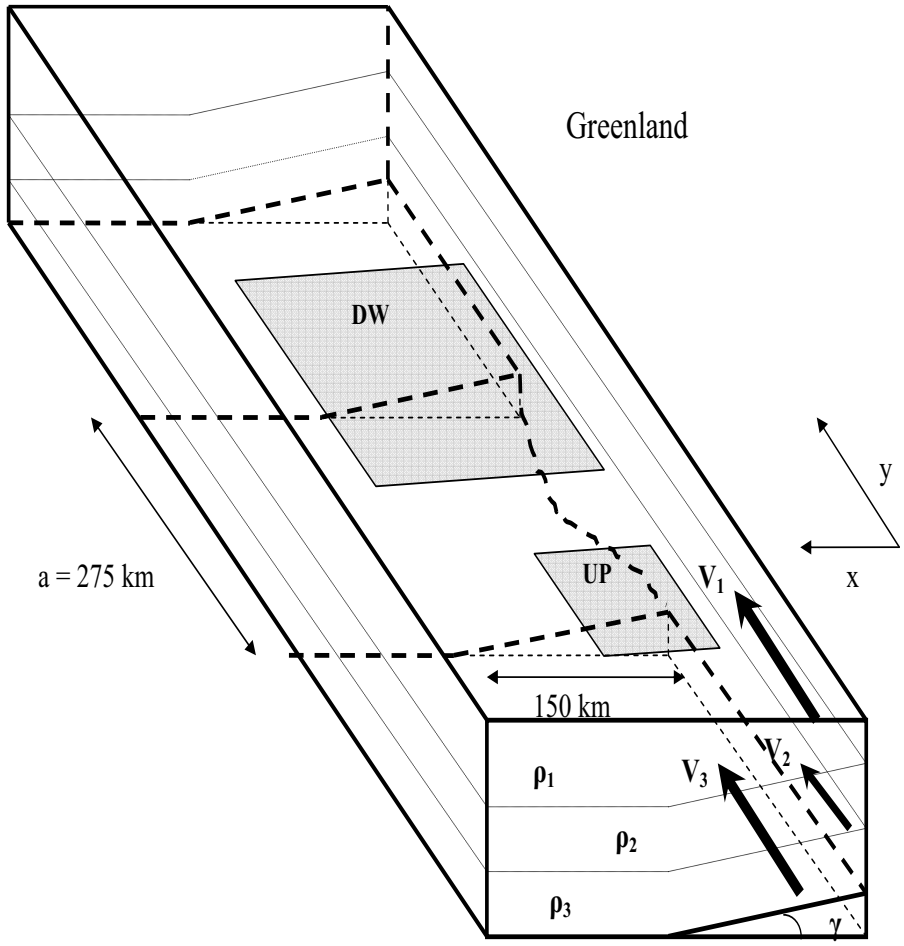

Figure 3: Schematic of the model geometry. The topography and the current configuration destabilizes the flow in the interval denoted by a. The shading boxes UP and DW indicate the two domains zoomed in Fig. 5. $x = 0$ along the eastern boundary.

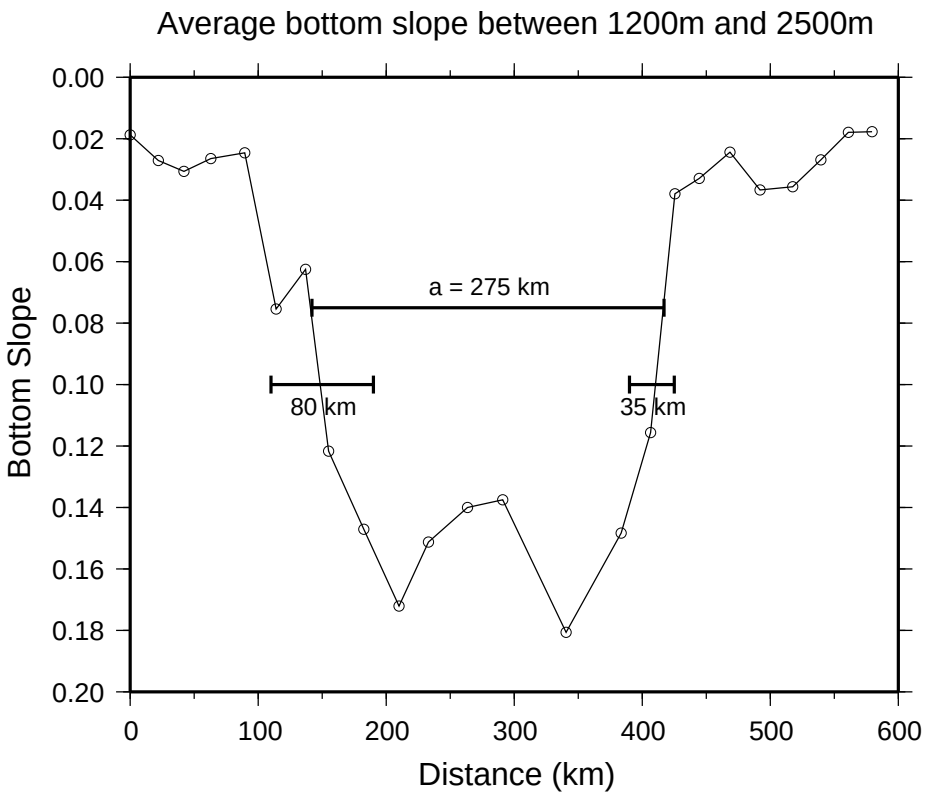
Average bottom slope between 1200m and 2500m
Bottom Slope
0.00
0.02
0.04
0.06
0.08
0.10
0.12
0.14
0.16
0.18
0.20
a = 275 km
80 km
35 km
0
100
200
300
400
500
600
Distance (km)

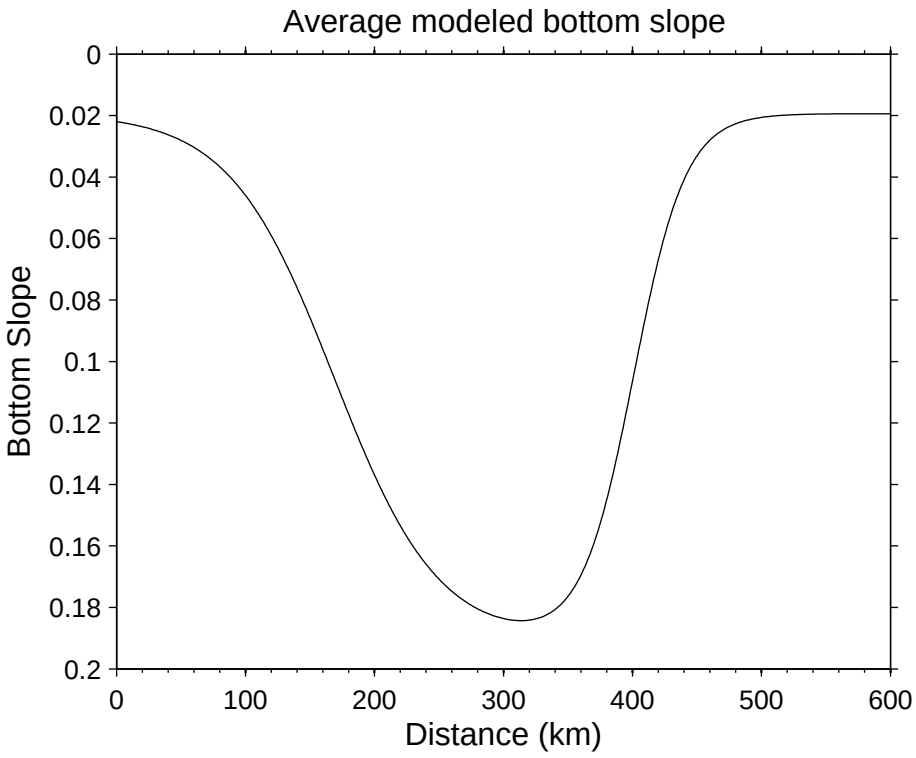

Figure 4: (a) Average bottom slope progressing northward along the continental slope of West Greenland, computed within the dashed box in Fig. 1. The scales used in the model are indicated. (b) The average bottom slope profile used in the model.

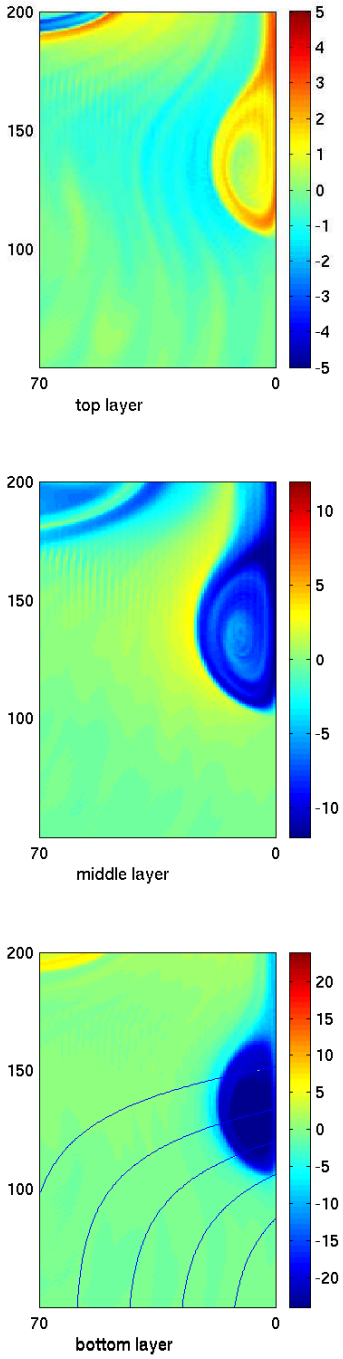

Figure 5: Zoomed in view of the potential vorticity disturbance in the upper, middle and lower layer with the isolines of the bathymetry overlaid in box *UP* in the schematic of Fig. 3, which corresponds to the interval 50-200 km in Fig. 4. The wall corresponding to "*Greenland*" is on the right (at $x = 0$) of each panel. The figure shows the formation of an anticyclone at the upstream step. Units are km for both axes.

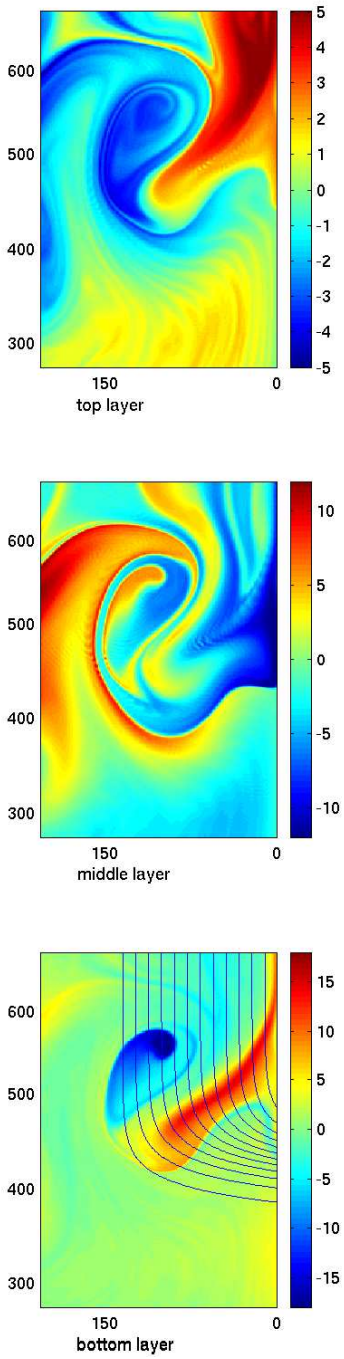

Figure 6: Zoomed in view of the potential vorticity disturbance in the upper, middle and lower layer with the isolines of the bathymetry overlaid in box DW in the schematic of Fig. 3, which occupies the interval 290-650 km in Fig. 4 and is about 4-times larger that the upstream box. The wall corresponding to "*Greenland*" is on the right (at $x = 0$) of each panel. The anticyclone formed at the upstream step and shown in Fig. 5 ten days later is detaching from the boundary and is forming a dipole. Units are km for both axes.